Glucose transporter 1-mediated vascular translocation of nanomedicines enhances accumulation and efficacy in solid tumors

Kazumi Suzuki, Yutaka Miura, Yuki Mochida, Takuya Miyazaki, Kazuko Toh, Yasutaka Anraku, Vinicio Melo, Xueying Liu, Takehiko Ishii, Osamu Nagano, Hideyuki Saya, Horacio Cabral, Kazunori Kataoka

PII: S0168-3659(19)30096-3
DOI: https://doi.org/10.1016/j.jconrel.2019.02.021
Reference: COREL 9660

To appear in: *Journal of Controlled Release*

Received date: 1 November 2018
Revised date: 6 February 2019
Accepted date: 17 February 2019

Please cite this article as: K. Suzuki, Y. Miura, Y. Mochida, et al., Glucose transporter 1-mediated vascular translocation of nanomedicines enhances accumulation and efficacy in solid tumors, Journal of Controlled Release, https://doi.org/10.1016/j.jconrel.2019.02.021

Glucose Transporter 1-Mediated Vascular Translocation of Nanomedicines Enhances Accumulation and Efficacy in Solid Tumors

Kazumi Suzuki[1,1,2], Yutaka Miura[1,1,3], Yuki Mochida[2], Takuya Miyazaki[1], Kazuko Toh[2], Yasutaka Anraku[1,2], Vinicio Melo[1,2], Xueying Liu[2], Takehiko Ishii[1,4], Osamu Nagano[3], Hideyuki Saya[3], Horacio Cabral[1,*] horacio@bmw.t.u-tokyo.ac.jp, Kazunori Kataoka[2,4,*] kataoka@pari.u-tokyo.ac.jp

[1]Department of Bioengineering, Graduate School of Engineering, The University of Tokyo, 7-3-1 Hongo, Bunkyo-ku, Tokyo 113-8656, Japan

[2]Innovation Center of Nanomedicine (iCONM), Kawasaki Institute of Industrial Promotion, 3-25-14 Tonomachi, Kawasaki-ku, Kawasaki 210-0821, Japan

[3]Division of Gene Regulation, Institute for Advanced Medical Research, School of Medicine, Keio University, 35 Shinanomachi, Shinjuku-ku, Tokyo 160-8582, Japan

[4]Policy Alternatives Research Institute, The University of Tokyo, 7-3-1 Hongo, Bunkyo-ku, Tokyo 113-0033, Japan

[*]Corresponding authors.

[1] These authors contributed equally.

[2] Present affiliation: JSR Corporation 25 Miyukigaoka, Tsukuba-shi, Ibaraki 305-0841 Japan.

[3] Present affiliation: Kowa Company, Ltd. 6-29, Nishiki 3-chome, Naka-ku, Nagoya, Aichi, 460-8625, Japan.

[4] Present affiliation: Research Division, NanoCarrier Co., Ltd, 144-15 Chuo, 226-39 Wakashiba, Kashiwa, Chiba, 277-0871, Japan.

ABSTRACT

Nanomedicine modification with ligands directed to receptors on tumor blood vessels has the potential for selectively enhancing nanomedicine accumulation in malignant tissues by overcoming the vascular barrier of tumors. Nevertheless, the development of broadly applicable ligand approaches capable of promoting the transvascular transport of nanomedicines in a wide spectrum of tumors has been elusive so far. By considering the indispensable and persistent glycolytic fueling of tumors, we developed glucose-installed polymeric micelles loading cisplatin (Gluc-CDDP/m) targeting the glucose transporter 1 (GLUT1), which is overexpressed in most tumors and present on vascular endothelial cells, toward improving the delivery efficiency and therapeutic efficacy. The design of the glucose ligands on Gluc-CDDP/m was engineered to control the conjugation *via* the carbon 6 of the glucose moieties, as well as the ligand density on the poly(ethylene glycol) (PEG) shell of the micelles. The series of micelles was then studied *in vitro* and *in vivo* against GLUT1-high human squamous cell carcinoma of the head and neck OSC-19 cells and GLUT1-low human glioblastoma-astrocytoma U87MG cells. Our results showed that precisely tuning the micelles to have glucose ligands on 25% of their PEG chains increased the efficacy against the tumors by significantly enhancing the tumor accumulation, even in GLUT1-low U87MG tumors. The enhancement of the intratumoral levels of these micelles was hindered by concomitant administration of glucose, or the GLUT1 inhibitor STF-31, confirming a GLUT1/glucose-mediated increment of the accumulation. Intravital confocal laser scanning microscopy imaging of tumor tissues further demonstrated the rapid extravasation and penetration of Gluc-CDDP/m in OSC-19 tumors compared to non-targeted CDDP/m. These findings indicate GLUT1-targeting as a promising approach for overcoming the vascular barrier and boosting the delivery of nanomedicine in tumors.

Keywords. Polymeric micelles, glucose, GLUT1, cisplatin, tumor vasculature, EPR effect.

INTRODUCTION

Nanomedicines have shown selective accumulation in tumors based on the enhanced permeability and retention (EPR) effect by exploiting the permeable vasculature and limited lymphatic drainage in cancerous tissues [1,2]. However, a limited fraction of the total administered dose reaches the tumor site by this route [3]. Moreover, in clinical tumors, the level of leaky vessels and extent of the EPR effect appear to be highly variable, which can limit the success of nanomedicines [4,5]. An attractive strategy for improving accumulation is circumventing the vascular barrier of tumors by promoting the translocation of nanomedicines through ligands directed to receptors on tumor blood vessels readily exposed to the bloodstream [6,7]. Nevertheless, despite this approach critically augmented nanomedicine levels in certain malignancies, such as cyclic RGD peptide-installed nanomedicines targeting $\alpha_V\beta_3$- and $\alpha_V\beta_5$-expressing vasculature in brain tumors [8,9] or iRGD peptide facilitated transport in tumors expressing neuropilin-1 (or neuropilin-2) on their endothelium [10], the development of ligand strategies promoting the transvascular transport of nanomedicines in a wide range of tumors remains to be satisfied, as the discovery of ubiquitous tumor vascular markers accessible *in vivo* has been exceptionally difficult.

Targeting receptors on tumor blood vessels that are involved in indispensable and persistent tumoral processes could provide an effective modality for broadly improving the delivery efficiency of nanomedicines. In this regard, glucose transporters, notably glucose transporter 1 (GLUT1), are crucial for the hallmark glycolytic fueling of tumors [11], as glucose cannot pass through cellular membranes by simple diffusion. Indeed, markedly increased accumulation of glucose has been reported in many human tumor types [12,13], with GLUT1

expression closely correlating with tumor malignancy and resistance to therapies [14-16]. Thus, several studies have used glucose as ligands [17], including glucose-installed nanomedicines [18,19], to target the glucose transporters on tumor cells. On the other hand, since the transport of glucose into tissues is mediated by GLUT1 on vascular endothelial cells [20,21], it is reasonable to assume the presence of GLUT1 in the tumor vasculature to satisfy the high glucose demand of cancer cells, thereby, representing a significant target for strategies aimed at enhancing transvascular transport. Nevertheless, such approach remains unexplored, as all previous studies on glucose-installed nanomedicines were aimed to target the tumor cell itself without focusing on the targeting of GLUT1 on the endothelial cells.

Here, we studied GLUT1-targeted nanomedicines as a new strategy directed to overcome vascular barrier, enhancing delivery and efficacy in solid tumors. These nanomedicines were prepared by controlled installation of glucose on polymeric micelles incorporating the antitumor agent cisplatin, which is used for the treatment of a wide range of tumors (**Figure 1**). The cisplatin-loaded micelles (CDDP/m) serving as the platform for this study have shown potent antitumor effects and reduced side effects in humans, and are being evaluated in Phase III clinical trials against pancreatic cancer [7,22]. Before evaluating the effects of GLUT1-targeting on these micelles, the expression of GLUT1 on the endothelial cells of tumor blood vessels was validated in xenografts and clinical tumor biopsies. Then, the ability of glucose-installed CDDP/m (Gluc-CDDP/m) to improve delivery efficiency through the glucose/GLUT1 system was compared *in vitro*, as well as *in vivo* against two tumor models, *i.e.* the high-GLUT1-expressing human squamous cell carcinoma of the head and neck (OSC-19), which harbor a large subpopulation of cisplatin-resistant cells with cancer stem-like cell characteristics [23], and the low-GLUT1-expressing human glioblastoma-astrocytoma (U87MG) [24]. Our results

demonstrated that precisely tuning the micelles to have 25% of their PEG chains with glucose conjugated at the carbon 6 *via* ether linkage promoted the selective accumulation in the tumors through GLUT1-associated vascular translocation. The intratumoral levels of these micelles in both GLUT1-high OSC-19 and GLUT1-low U87-MG tumors were 2-fold higher than those of the control CDDP/m in these tumors, which are solely based on the EPR effect, allowing Gluc-CDDP/m to improve the antitumor activity. These findings indicate our approach of exploiting the GLUT1/glucose interaction by glucose-installed nanomedicines as a promising new strategy for boosting delivery and efficacy of nanomedicines against solid tumors.

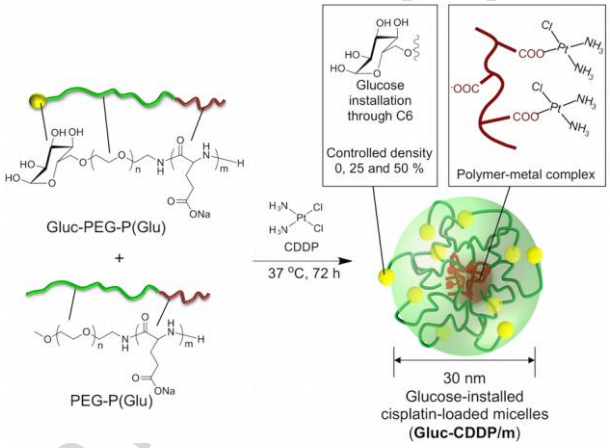

Figure 1. Construction of glucose-installed cisplatin-loaded micelles (Gluc-CDDP/m) from poly(ethylene glycol)-poly(L-glutamic acid) (PEG-P(Glu); MW_{PEG} = 12 kDa; polymerization degree of P(Glu) = 40) and α-glucopyranos-6-*O*-yl-poly(ethylene glycol)-poly(L-glutamic acid) (Gluc-PEG-P(Glu); MW_{PEG} = 12 kDa; polymerization degree of P(Glu) = 40) block copolymers. Glucose was installed through carbon 6 into the α-end of the poly(ethylene glycol) (PEG) block *via* ether linkage. The micelles were self-assembled by the polymer-metal complex formation between the carboxylate group in the P(Glu) segment and cisplatin. The density of glucose on the

surface of the micelles was controlled through the mixing ratio of Gluc-PEG-P(Glu) and CH_3O-PEG-P(Glu).

MATERIALS AND METHODS

Materials

1,2-O-isopropylidene-α-D-glucofuranose (MIG), 2,2-dimethoxypropane, *p*-toluenesulfonic acid monohydrate were purchased from Tokyo Chemical Industries, Ltd., (Tokyo, Japan). Dimethyl sulfoxide (>99%), triethylamine (TEA, >99%), pyridine (>99%), tetrahydrofuran (THF, >99%), and methanesulfonyl chloride (MsCl, >99%) were purchased from Wako Pure Chemical Industries, Ltd., (Tokyo, Japan), purified by distillation over drying agents, *e.g.*, CaH_2 or P_2O_5, and were transferred under argon. Ethylene oxide (Sumitomo Seika Chemical, Osaka, Japan) was dried over CaH_2 and distilled under an argon atmosphere. Potassium naphthalene was prepared as a THF solution according to a previous paper [25]. α-Methoxy-ω-amino-poly(ethylene glycol) (MeO-PEG-NH_2, 12,000 g/mol, NOF Corporation, Tokyo, Japan) was purified using an ion exchange CM Sephadex C-50 column (GE Healthcare Ltd., UK). Pivaloyl chloride (Tokyo Chemical Industries, Ltd., Tokyo, Japan), ammonia solution (ca. 28%, Nakarai Tesque, Kyoto, Japan), cis-dichlorodiamineplatinum (II) (cisplatin, Aldrich Chemical Co., Inc. Milwaukee, WI), *N*-carboxy anhydride of γ-benzyl L-glutamate (Chuo Kaseihin Co., Inc., Tokyo, Japan), Alexa 674-succinimidyl ester (Life Technologies Corporation, Tokyo, Japan), Alexa 555-succinimidyl ester (Life Technologies Corporation, Tokyo, Japan), and other reagents were used without further purification. Dulbecco's modified eagle's medium (DMEM) and STF-31 (4-[[[[4-(1,1-Dimethylethyl)phenyl]sulfonyl]amino]methyl]-N-3-

pyridinyl-benzamide) were obtained from Sigma-Aldrich Co. (ST. Louis, MO) and Thermo Fisher Scientific Inc. (Waltham, MA). Fetal bovine serum (FBS) was purchased from Dainippon Sumitomo Pharma Co., Ltd. (Osaka, Japan). Phosphate-buffered saline (PBS) was purchased from Wako Pure Chemical Industries Ltd. (Osaka, Japan). Anti-CD31 monoclonal antibody, anti-mouse IgG AlexaFluor488 and anti-mouse IgG AlexaFluor647 were purchased from Abcam (Cambridge, UK), while anti-GLUT1 antibody was bought from Cosmo Bio Co., Ltd (Tokyo, Japan). Tissue arrays of human head and neck cancer, and brain tumors were purchased from Biomax (Rockville, MD). AlexaFluor555- and AlexaFluor647-NHS esters were purchased from Thermo Fischer Scientific, Waltham, MA.

Cell lines and animals.

Human glioblastoma-astrocytoma (U87MG) cells, human colorectal carcinoma (HT29), and triple negative breast cancer cells (MDA-MB-231) were purchased from ATCC (Manassas, VA). Human squamous cell carcinoma cells (OSC-19) were obtained from Kanazawa University. These cell lines were grown in Dulbecco's Modified Eagle's Medium (DMEM) plus 10 % FBS in a humidified atmosphere containing 5 % CO_2 at 37 ^{o}C. BALB/C nu/nu female mice (female; body weight, 18-20 g; age, 6 weeks) were obtained from Oriental Yeast Co., Ltd. and were allowed to acclimatize for 7 days before inoculation of tumors. The animal experiments were performed in accordance with the Guidelines for the Care and Use of Laboratory Animals as stated by The University of Tokyo, as well as by the Animal Care and Use Committee of the Innovation Center of Nanomedicine.

Tumor models

The tumors were prepared by subcutaneous inoculation of OSC-19 ($1x10^6$ cells/mouse) and U87MG ($1x10^6$ cells/mouse). The tumors were allowed to grow to approximately 50 mm^3 for the antitumor activity experiments, and 100 mm^3 for the evaluation of the tumor accumulation of free CDDP and the series of micelles. For the histological analysis, not only OSC-19 and U87MG tumors were prepared, but also subcutaneous tumors HT-29 and MDA-MB-231 after inoculating $1x10^6$ cells/mouse. The tumors for the histology evaluation were grown until they reached 100 mm^3.

Assessment of GLUT1 and CD31 colocalization by immunofluorescence

To study the presence of GLUT1 on the tumor vasculature, the tumors were collected and fixed with 4% formaldehyde, incubated in 30% sucrose and embedded in Tissue-Tek OCT Compound (Sakura-finetek Japan). Sections from each tumor were cut by a Cryostat (Leica CM1950), and stained for GLUT1 by using anti-GLUT1 mouse antibody, which also cross-reacts with human GLUT1, and endothelial cells of tumors by using anti-CD31 antibody, with fluorescent secondary antibodies. Moreover, GLUT1 and CD31 were also stained in the tissue arrays of human head and neck cancer, and brain tumors after retrieving the antigens. The samples were imaged by using a confocal laser-scanning microscope (LSM780 Meta, Zeiss; Germany). The colocalization of CD31 with GLUT1 was determined by using ImageJ in 3 samples of the murine xenografts, and 6 samples in the human tissue arrays.

Measurements

Nuclear magnetic resonance spectra were recorded using JEOL JNM-ECS400 (400 MHz for ^{1}H and 100 MHz for ^{13}C) instruments with $CDCl_3$, *d*-DMSO, and D_2O containing 0.05% tetramethylsilane or trimethylsilyl propanoic acid at 22 ^{o}C. Size exclusion chromatography (SEC), which is a chromatographic technique that allows the separation of molecules in solution based on their size, was used to determine the polydispersity index (PDI; M_w/M_n) of the molecular weight of the block copolymers. SEC was performed at 40 °C using a Tosoh HLC-8220 GPC system equipped with a TSKgel G3000HHR column (linear, 7.8 mm × 300 mm; pore size, 7.5 nm; bead size, 5 μm; exclusion limit, 6×10^4 g/mol), a TSKgel G4000HHR column (linear, 7.8 mm × 300 mm; pore size, 20 nm; bead size, 5 μm; exclusion limit, 4×10^5 g/mol), and a TSKgel guard column H_{HR}-L in DMF containing lithium bromide (10 mM) at a flow rate of 0.5 mL/min. The number-averaged molecular weight (M_n) and PDI (M_w/M_n) of PEG derivatives were calculated on the basis of the PEG calibration. The sizes of the polymeric micelles were measured using zetasizers (Malvern Zetasizer Nano ZS90) equipped with a 4.0 mW He–Ne laser operating at 633 nm with 90° collecting optics. The zeta potential values of the micelles were determined by laser Doppler electrophoresis in 10 mM phosphate buffer (pH 7.4) by using Zetasizer. Data were analyzed using Malvern Dispersion Technology 4.20. Platinum concentration of the micelles was determined by inductively coupled plasma-mass spectrometry (ICP-MS) using a 7700x ICP-MS (Agilent Technologies, Santa Clara, CA; RF power, 1550 W; sampling depth, 8.0 mm; plasma gas current, 16 L/min; carrier gas flow rate, 1.02 L/min; peristaltic pump, 0.10 rps; monitoring mass, 195 (Pt); integration interval, 0.1 s; sampling period, 0.31 s). Microscopic images of the micelles were obtained by transmission electron microscopy (TEM; JEOL, Japan) at an accelerating voltage of 75 kV. The sample solutions (2 μL) were

dropped onto a 400 mesh copper grids, and stained by deposition of a drop of an aqueous solution of 50% ethanol and 2-wt% uranyl acetate. The size distribution of the micelles was analyzed from the TEM images by using ImageJ.

Synthesis of 1,2-*O*-Isopropylidene-6-*O*-pivaloyl-α-D-glucofuranose (6-Piv-MIG)

MIG (25.0 g, 113.5 mmol) was dissolved in dry pyridine (150 mL) and pivaloyl chloride (13.7 g, 113.6 mmol) was slowly added. Then, the mixture was stirred for 5 h at room temperature. The solvent was evaporated to dryness and the residue was washed with water, and filtered to obtain the crude product as solid. The crude product was dried under vacuum, and then purified by recrystallization from ethyl acetate. Yield: 28.4 g (82.3 %); R_f = 0.25 (dichloromethane:methanol = 9 :1 (*v*/*v*)); mp 145-147 ^{o}C; ^{1}H NMR (400 MHz, $CDCl_3$): δ 5.96 (d, J =3.2 Hz, 1H), 4.55 (d, J = 3.6 Hz, 1H), 4.44 (dd, J = 5.6 Hz, J = 13.6 Hz 1H), 4.36 (d, J = 2.0 Hz, 1H), 4.26-4.21 (m, 2H), 4.08 (dd, J = 2.8 Hz, J = 6.0 Hz 1H), 1.48 (s, 3H), 1.32 (s, 3H), 1.23 (s, 9H); ^{13}C NMR (100 MHz, $CDCl_3$): δ 179.4, 111.8, 104.9, 85.1, 79.2, 75.4, 69.1, 66.1, 38.9, 27.1, 26.8, 26.2; The other characteristic data were matched with the literature data.

Synthesis of 1,2:3,5-Di-*O*-isopropylidene-6-*O*-pivaloyl-α-D-glucofuranose (6-Piv-DIG(6))

A mixture of 6-Piv-MIG (20.0 g, 65.7 mmol), *p*-toluenesulfonic acid monohydrate (500 mg, 2.90 mmol) and 2,2-dimethoxypropane (40 mL) was refluxed for 1 h. After 2,2-dimethoxypropane was evaporated to dryness, the residue was dissolved to dichloromethane, and was washed twice with saturated $NaHCO_3$ and three times with brine. The dichloromethane layer

was dried with anhydrous Na_2SO_4. After the solvent was removed by evaporator, the crude product was purified by column chromatography on silica gel with hexane/ethyl acetate gradient system (from 1/0 to 7/3 (*v*/*v*)) to give 6-Piv DIG(6) as a white solid. Yield: 10.3 g (45.5 %); R_f = 0.81 (hexane : ethyl acetate = 7:3 (*v*/*v*)); ^{1}H NMR (400 MHz, $CDCl_3$): δ 6.00 (d, J = 3.6 Hz, 1H), 4.58 (d, J = 4.0 Hz, 1H), 4.31 (dd, J = 3.2 Hz, J = 12.0 Hz, 2H), 4.21 (d, J = 3.6 Hz, 1H), 4.21-4.14 (m, 1H), 3.78 (m, 1H), 1.61 (s, 1H), 1.45 (s, 3H), 1.35 (s, 1H), 1.34 (d, J = 3.2 Hz, 2H), 1.21 (s, 9H); ^{13}C NMR (100 MHz, $CDCl_3$): δ 178.1, 112.2, 106.4, 101.0, 83.9, 79.5, 75.0, 70.3, 64.1, 38.8, 27.2, 26.6, 24.0, 23.8; The other characteristic data were matched with the literature data.

Synthesis of 1,2:3,5-Di-*O*-isopropylidene-α-D-glucofuranose (DIG(6)) (Figure S1A)

A solution of 6-Piv DIG(6) (5.0 g, 14.5 mmol) in methanol (100 mL) including 1 M sodium methoxide was stirred during 24 h. The reaction mixture was neutralized by addition of dry ice. The mixture was extracted three times with dichloromethane, dried with anhydrous Na_2SO_4, filtered, and evaporated. The oily residue was purified by flash chromatography (hexane/ethyl acetate, 3:2 *v*/*v*, R_f = 0.29) to afford DIG(6). Yield: 2.80 g (74.1 %). ^{1}H NMR (400 MHz, $CDCl_3$): δ 6.00 (d, J = 4.0 Hz, 1H), 4.59 (d, J = 3.6 Hz, 1H), 4.38 (dd, J = 3.6 Hz, J = 7.2 Hz, 1H), 4.19 (d, J = 3.6 Hz, 1H), 3.87-3.82 (m, 1H), 3.72-3.63 (m, 1H), 2.03 (t, J = 6.4 Hz, 1H), 1.49 (s, 3H), 1.37 (s, 6H), 1.33 (s, 3H); ^{13}C NMR (100 MHz, $CDCl_3$): δ 112.2, 106.4, 101.0, 84.0, 79.0, 75.0, 63.4, 27.1, 26.5, 24.1, 24.0; The other characteristic data were matched with the literature data.

Polymerization of ethylene oxide (Figure S1B)

A typical polymerization of ethylene oxide (EO) was carried out under an argon atmosphere according to a previously reported method with a minor modification [26]. Briefly, the pre-dried glucose-based initiator, DIG(6) (390 mg, 1.50 mmol), potassium naphthalene (1.50 mmol), and dry THF (100 mL) were added into a reaction glassware equipped with a three-way stopcock. After stirring for 15 min, EO (18.9 g, 428 mmol) was added to the solution *via* a cooled cannula. The polymerization was carried out at 25 ^{o}C. The polymerization mixture was poured into a large amount of diethyl ether. The precipitate was purified by reprecipitation with dichloromethane/diethyl ether and then dried in vacuo to give α-DIG(6)-ω-hydroxy-PEG (17.0 g, yield = 98 %) in a 99 % conversion. The M_n and M_w/M_n values were 12800 g/mol and 1.03, respectively. ^{1}H NMR (400 MHz, $CDCl_3$): δ 5.99 (d, J = 3.6 Hz, 1H), 4.57 (d, J = 3.6 Hz, 1H), 4.32 (dd, J = 3.6 Hz, J = 7.6 Hz, 1H), 4.19 (d, J = 3.6 Hz, 1H), 3.90-3.34 (m, 1086H), 1.49 (s, 3H), 1.37 (s, 3H), 1.36 (s, 3H), 1.32 (s, 3H).

Preparation of α-DIG(6)-ω-amino-poly(ethylene glycol) (DIG(6)-PEG-NH_2) (Figure S1B)

α-DIG(6)-ω-amino-poly(ethylene glycol) was synthesized as described previously [26]. Briefly, a solution of MsCl (0.32 mL, 14.1 mmol) in THF (200 mL) was dropwisely added into a mixture of TEA (0.89 mL, 6.39 mmol) and DIG(6)-PEG-OH (19.0 g, 1.48 mmol) in THF (120 mL). The reaction mixture was stirred in a dry argon atmosphere at 0 °C for 30 min and at room temperature for overnight. The solution was concentrated and poured into a large amount of cold diethyl ether. The precipitate was purified by reprecipitation with dichloromethane/diethyl ether, and dried under reduced pressure to yield α-DIG(6)-ω-methanesulfonyl-terminated poly(ethylene

glycol) (DIG(6)-PEG-Ms; Yield = 93 %, ^{1}H NMR (400 MHz, $CDCl_3$): δ 5.99 (d, J = 3.6 Hz, 1H), 4.57 (d, J = 3.6 Hz, 1H), 4.39-4.37 (m, 2H), 4.32 (d, J = 3.6 Hz, J = 7.2 Hz, 1H), 4.20 (d, J = 3.6 Hz, 1H), 3.89-3.40 (m, 1090H), 3.09 (s, 2H), 1.49 (s, 3H), 1.37 (s, 3H), 1.36 (s, 3H), 1.32 (s, 3H)). Then, DIG(6)-PEG-Ms (15.0 g, 1.17 mmol) was dissolved in 28% NH_3 aq. (150 mL) and stirred for 3 days at room temperature. The solution was concentrated by evaporation and then dialyzed against distilled water, followed by lyophilization to yield α-DIG(6)-ω-amino-poly(ethylene glycol) (DIG(6)-PEG-NH_2). The obtained DIG(6)-PEG-NH_2 was further purified with an ion-exchange CM Sephadex C-50 column (GE Healthcare UK Ltd., Buckinghamshire, UK) before use. Yield = 89 %, Conv.$_{-NH2}$ = 97 %, M_n = 12,900, M_w/M_n = 1.04. ^{1}H NMR (400 MHz, $CDCl_3$): δ 5.99 (d, J = 3.6 Hz, 1H), 4.57 (d, J = 3.6 Hz, 1H), 4.32 (dd, J = 4.0 Hz, J = 7.6 Hz, 1H), 4.20 (d, J = 3.6 Hz, 1H), 3.92 (t, J = 4.8 Hz, 2H), 3.81-3.45 (m, 1090H), 3.17 (t, J = 4.8 Hz, 2H), 1.49 (s, 3H), 1.37 (s, 3H), 1.36 (s, 3H), 1.33 (s, 3H).

Preparation of α-glucopyranos-6-*O*-yl-poly(ethylene glycol)-poly(L-glutamic acid) block copolymer (Gluc-PEG-P(Glu)) (Figure S1B)

A typical procedure for the polymerization of *N*-carboxy anhydride of γ-benzyl L-glutamate is as follows: A solution of *N*-carboxy anhydride of γ-benzyl L-glutamate (0.471 g, 1.79 mmol) in DMSO (15.0 mL) and a solution of DIG(6)-PEG-NH_2 (0.494 g, 0.0388 mmol) in DMSO (40.0 mL) were combined and stirred in a dry argon atmosphere at 25 °C. After 72 h, the solution was poured into a large amount of cold diethyl ether. The precipitate was purified by reprecipitation with dichloromethane/diethyl ether, and dried under reduced pressure to yield α-DIG(6)-poly(ethylene glycol)-poly(γ-benzyl L-glutamate) (DIG(6)-PEG-PBLG; yield = 89%, M_n

= 21,700; M_w/M_n = 1.07; NMR (400 MHz, *d*-DMSO): δ 7.39-7.10 (m, 190H), 5.93 (d, J = 3.6 Hz, 1H), 5.20-4.80 (m, 76H), 4.54 (d, J = 3.6 Hz, 1H), 4.40-4.20 (m, 39H), 4.13 (d, J = 3.6 Hz, 1H), 3.90 (br, 2H), 3.80-3.30 (m, 1090H), 2.70-1.70 (m, 154H*), 1.39 (S, 3H), 1.31 (s, 3H), 1.28 (s, 3H), 1.26 (s, 3H) (*Due to peak overlapping with DMSO, the proton number was calculated by NMR result performed with $CDCl_3$). To deprotect benzyl groups on polymer backbone, the obtained block copolymer was stirred in 0.5 N NaOH aq. (31 mL) for overnight at room temperature. The polymer was purified in water using a dialysis membrane (Spectra/Pro 6 Membrane: MWCO, 3500), followed by lyophilization to yield DIG(6)-PEG-P(Glu). To deprotect isopropylidene acetal groups, the DIG(6)-PEG-P(Glu) was stirred in TFA aq. (water/TFA = 1/4, *vol*/*vol*, 10 mL) for 30 min at room temperature. The polymer was purified in water using a dialysis membrane (Spectra/Pro 6 Membrane: MWCO, 3500), followed by lyophilization to yield α-glucopyranos-6-*O*-yl-PEG-P(Glu) (Gluc-PEG-P(Glu): Yield = 89%, M_n = 18,100, M_w/M_n = 1.09. ^{1}H NMR (400 MHz, D_2O with TMS): δ 5.26 (m, 1H), 4.50-4.24 (m, 38H), 4.25-4.08 (m, 4H), 4.05-3.30 (m, 1094H), 3.17 (m, 1H), 2.60-1.70 (m, 156H).

Preparation of glucose-installed cisplatin-loaded micelles (Gluc-CDDP/m)

Cisplatin-loaded polymeric micelles were prepared according to the previously described synthetic method with a slight modification [27,28]. The glucose densities on the micelles were tuned to 0, 25 and 50% by controlling the ratio between MeO-PEG-P(Glu), and Gluc-PEG-P(Glu) block copolymers, resulting in micelles with 0, 25 and 50% of the number of their PEG chains modified with glucose moieties. For example, the typical procedure for the preparation of α-glucopyranos-6-*O*-yl-conjugated micelles (Gluc-CDDP/m) containing 25 mol% glucose

residues on their surface was as follows: a solution of CDDP (16.5 mg, 0.055 mmol) in water (10.2 mL) was stirred for 1 h at 50 °C. The obtained solution (10 mL) was filtered using a membrane (pore size, 0.22 μm) and added to a reaction vial containing MeO-PEG-P(Glu) and Gluc-PEG-P(Glu) ([Glu] = 5 mmol/L, [CDDP]/[Glu] = 1.0 (mol/mol), [MeO-PEG-P(Glu)]/[Gluc-PEG-P(Glu)] = 0.75/0.25 (mol/mol)). The reaction mixture was stirred for 120 h at 37 °C, and then purified by dialysis using the cellophane tube (Spectra/Pro 6 Membrane: MWCO, 3500). The micelle stability and drug release were evaluated by DLS, and by the dialysis method in 10 mM PBS plus 150 mM NaCl at 37 °C, respectively.

***In vitro* cytotoxicity assay**

OSC-19 or U87MG spheroid arrays were prepared by culturing these cells in DMEM containing 10% FBS on a 96-well micro-patterned multiplate designed for spheroid preparation, Cell-able (Toyo Gousei Co., Ltd., Tokyo, Japan, 2.0×10^4 cells/well). Stable spheroid arrays are confirmed to form after 4 days of culture, and subsequently, they were incubated with free CDDP or the series of polymeric micelles at different CDDP-based concentrations ranging from 100- to 0.001-μM. After 6 h incubation, the spheroids were washed with fresh medium, and post-incubated for 60 h. The 50% growth inhibitory concentrations (IC_{50}) were evaluated by a CellTiter-Glo 3D Cell Viability Assay kit (Promega Corporation, Madison, USA), following the manufacturer's protocol. In addition, the GLUT1 in OSC-19 cells was knocked down by using Dharmacon's lentiviral shRNA kit (Horizon; Cambridge, UK) by following the specifications of the provider for producing cells without GLUT1 as a negative control. These GLUT1(-) OSC-19 cells were used to prepare spheroids, and the cytotoxicity of free CDDP or the series of

polymeric micelles was studied as described above. The experiments were repeated 4 times, and the average IC_{50} values were calculated.

Antitumor activity

To evaluate the antitumor efficacy, BALB/c nude mice (Oriental Yeast Co., Ltd., Tokyo, Japan) bearing OSC-19 or U87MG subcutaneous tumor (n = 6) were treated 4 times intravenously every four days with 1 mg/kg (on a CDDP basis) of polymeric micelles. The tumor size (V) was estimated using the following equation: $V = a \times b^2/2$, where a and b are the major and minor axes of the tumor measured by using a caliper. Student's t-test was used to analyze the significance in the tumor volume between the experimental and control groups. $P < 0.05$ was considered statistically significant in each analysis. In addition, the body weight of mice was followed during the experiment.

Plasma clearance and biodistribution of free CDDP and polymeric micelles

To evaluate the plasma clearance and biodistribution, BALB/c nude mice bearing OCS19 tumors (n = 6) were intravenously injected with a series of polymeric micelles or free CDDP at 100 μg/mouse on a CDDP basis. Tumors were removed at 0.2, 1, 4, 8 and 24 h after injection, washed with PBS, and decomposed with concentrated nitric acid at 200 °C. The dried samples were dissolved in 1 vol.% nitric acid (1.0 mL), and the platinum concentrations were measured by ICP-MS. For analysis of plasma clearance, blood was collected from the inferior vena cava, heparinized, and centrifuged to obtain the plasma. These plasma samples were treated with nitric acid as described above and analyzed by ICP-MS. Moreover, the inhibition of the accumulation of the Gluc-25%-CDDP/m was done by intraperitoneally injecting a 50 wt% glucose solution (200 μL) in OSC-19 tumor-bearing mice before and 30 min after the micelle administration, or

by intraperitoneally injecting the GLUT1 inhibitor STF-31 (15 mg/kg; 50 μL) at 48 h, 24 h and 5 min before the micelle administration. The tumors were collected at 1 and 4 h after the micelle injection, and the drug concentration in the tissues was analyzed as described above.

Intravital microscopy

For this experiment, we prepared fluorescent labeled micelles. Thus, Alexa 647-NHS or Alexa 555-NHS were conjugated to the primary amino group at the end of the poly(amino acid) segment of α-CH_3O-PEG-P(Glu) block copolymer. The fluorescent labeled polymers were purified by using disposable PD10 columns. Then, CDDP/m were prepared by using Alexa 647-labeled α-CH_3O-PEG-P(Glu) block copolymers, while Gluc-25%-CDDP/m were prepared by using 75% of Alexa 555-labeled α-CH_3O-PEG-P(Glu) and 25% of Gluc-PEG-P(Glu) block copolymers. The intravital CLSM was performed according to the previously reported method [29]. OSC-19 tumors were grown subcutaneously until they reached 100 mm^3. The tumors were then exposed by making a 4-cm surgical incision without damaging the vessels in the surroundings. Then, the skin flap covering the tumor was folded and the tumor was set under the objective lenses of a Nikon A1R CLSM system connected to an upright ECLIPSE FN1 (Nikon, Japan). Ten minutes before imaging, the mice received an intravenous injection of 100 μL Hoechst (1 mg/mL) to stain the nuclei of the cells in the tumors. Then, Alexa 647-labeled CDDP/m and Alexa 555-labeled Gluc-25%-CDDP/m at a dose of 10 mg/kg on a CDDP basis were intravenously co-injected *via* the tail vein. The Alexa 647-labeled CDDP/m and the Alexa 555-labeled Gluc-25%-CDDP/m were detected by using 633/670 nm and 560/620 nm

excitation/emission filters, respectively. Time-lapse snapshots of the tumor were taken every 15 min for 3 h. The images were then analyzed by using ImageJ.

RESULTS

Expression of GLUT1 on tumor vasculature

The expression of GLUT1 on the endothelial cells of the blood vessels of tumors was first studied to validate the availability of the target *in vivo*. Thus, we performed immunofluorescence staining of GLUT1 (**Figure 2A-C; green**) and CD31 (**Figure 2A-C; red**) in tissue samples from both OSC-19 and U87MG tumors, as well as from tissue microarrays of human head and neck tumors, and brain tumors, by using anti-GLUT1 and anti-CD31 antibodies, and fluorescent-labeled secondary antibodies. The colocalization of GLUT1 and CD31 is shown in yellow color in the microscopic images (**Figure 2A-C**). The histology analysis demonstrated high colocalization of GLUT1 and CD31 in the tumor models (**Figure 2A and 2B)**, with a colocalization ratio of approximately 90% (**Figure 2D**). It is also worth noting the contrasting GLUT1 expression in OSC-19 and U87MG tumors, as shown by the GLUT1 staining of the interstitium of the tumors (**Figure 2A and 2B; green**). In the human tissue array samples, a high level of colocalization between GLUT1 and CD31 was detected, which corresponded with the observations in the murine tumor models (**Figure 2C and 2D**). Interestingly, benign head and neck lesions (Schwannomas) showed less GLUT1 expression both in the blood vessels and in the interstitium (**Figure 2C and 2D**). In addition, the colocalization of GLUT1 and CD31 was detected in xenografts of colon (HT-29) and breast (MDA-MD-231) cancers (**Supplementary Figure S2**). Thus, these results underline the occurrence of GLUT1 in the vessels of tumors, and

suggest the potential of GLUT1 as a target for glucose-installed nanomedicines directed to overcome the vascular barrier.

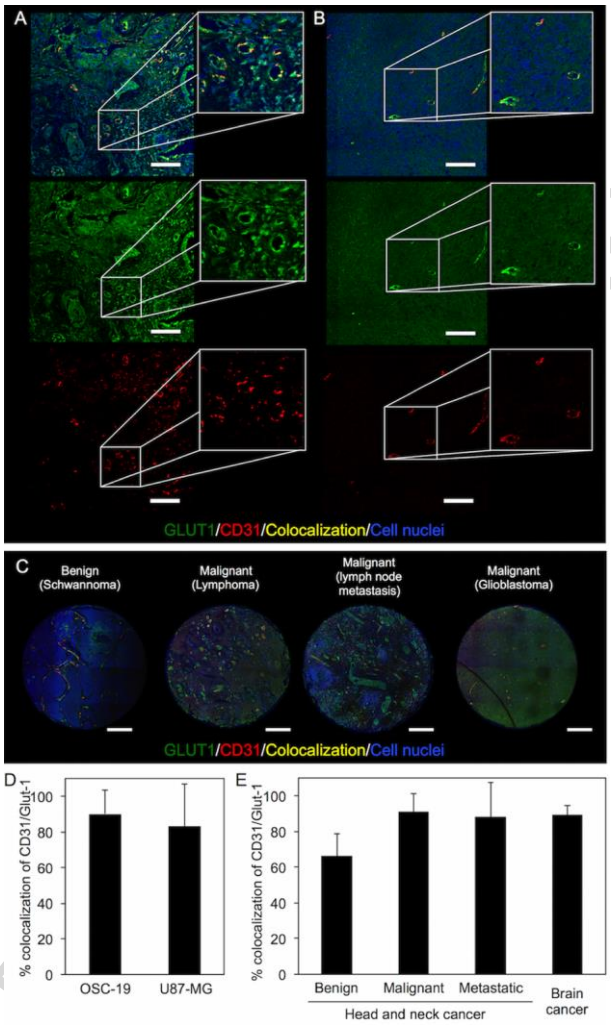

Figure 2. Colocalization of blood vessels (red) and GLUT1 (green) in murine tumor models and tissue microarrays of human tumors, determined by fluorescence immunohistochemistry. A. Murine model of high-GLUT1-expressing human squamous cell carcinoma of the head and neck (OSC-19). B. Murine model of glioblastoma-astrocytoma (U87MG). Scale bar = 100 µm. C. Representative human tissues of head and neck tumor and brain tumors. Scale bar = 500 µm. D. Quantification of colocalization of CD31 and GLUT1 in the mouse tumor models. Data are shown as the mean ± S.D. (n = 3). E. Quantification of colocalization of CD31 and GLUT1 in

the human samples. Data are shown as the mean ± S.D. (n = 6). The cell nuclei were stained by using Hoechst (blue).

Construction of glucose-installed cisplatin-loaded micelles

Motivated by the presence of GLUT1 in the lumen of the tumor vessels, we proceeded to develop CDDP/m having glucose moieties on their surface. It is important to note that the design of the glucose ligands to enhance cell uptake and *in vivo* delivery should consider the structural features of GLUTs for avoiding modifications on the hydroxyls of glucose implicated in hydrogen bonding interactions with the transporters [17]. Previous reports indicate that the hydroxyl groups at carbon 1 and carbon 3, as well as the pyran oxygen 5 in the closed conformation of glucose, are involved in stabilizing hydrogen bonds with the amino acid residues in GLUT1 [30,31], while the hydroxyl groups of glucose at carbon 2, carbon 4 and carbon 6 are less related to the recognition of glucose by GLUT1. Thus, in this study, we prepared acetalized glucose-installed PEG (Mw: 12,000) *via* the carbon 6 position (DIG(6)-PEG) through ring-opening polymerization of ethylene oxide by using a glucose-based initiator (potassium salt of DIG(6)) (**Figure 1 and Supplementary Figure S1**). Hydroxy group at the ω-end of DIG(6)-PEG was subsequently functionalized to primary amino group to initiate the ring opening polymerization of *N*-carboxy anhydride of γ-benzyl L-glutamate for preparing DIG(6)-PEG-poly(γ-benzyl L-glutamate) block copolymer (DIG(6)-PEG-PBLG). Acetal groups in DIG(6) as well as benzyl groups in the side chain of DIG(6)-PEG-PBLG were then deprotected to obtain Gluc-PEG-poly(glutamic acid) block copolymer (Gluc-PEG-P(Glu)). Degree of

polymerization (DP) of Glu units in the block copolymers was adjusted in the range of 36~38. The characteristics of the Gluc-PEG-P(Glu) are summarized in **Supplementary Table 1**.

A series of Gluc-CDDP/m with varying degree of glucose density on their surface (0, 25 and 50 mol%) were prepared by adjusting the ratio of Gluc-PEG-P(Glu) and α-CH_3O-PEG-P(Glu) block copolymers, and mixing with cisplatin in aqueous solution (**Figure 1**). The micelles were self-assembled in aqueous milieu after the formation of coordination bonds between the carboxylate groups in the block copolymers and the Pt atom in cisplatin (**Figure 1**) [27,28]. The diameter and surface charge of the Gluc-CDDP/m were found to be comparable to those of non-functionalized CDDP/m (CDDP/m), *i.e.* approximately 30 nm with similar size distribution (**Supplementary Figure S3**), and close to neutral, respectively (**Table 1**). Moreover, TEM analysis of the micelles was done after negative staining with 2-wt% uranyl acetate. The TEM images showed that CDDP/m and Gluc-CDDP/m present comparable spherical morphology and narrow size distribution with an average diameter of approximately 14 nm (**Supplementary Figure S4**). It is worth noting that the PEG shell is not visible after uranyl acetate staining by TEM, suggesting that the size distribution obtained from the TEM images corresponds to that to the core of the micelles. In addition, all the micelles showed a comparable drug loading of approximately 30% in weight (**Table 1**).

Table 1. Structural features of the series of polymeric micelles

Micelle	Glucose density (% of total PEG chains)	Size[a] (nm)	PDI[a]	Z-potential (mV)[b]	Drug loading (%weight)[c]
CDDP/m	0	31	0.13	-3.1	29
Gluc- CDDP/m	25	29	0.13	-3.2	31

50	28	0.13	-1.4	29

[a]Determined by dynamic light scattering.
[b]Determined by laser Doppler electrophoresis in 10 mM phosphate buffer (pH 7.4)
[c]Determined by inductively coupled plasma-mass spectrometry.

The stability of the micelles was evaluated in physiological saline (10 mM PBS plus 150 mM NaCl) at 37 °C by following the changes in the size, PDI and scattering light intensities. The size and polydispersity index of all the micelles was maintained throughout the experiment (**Figure 3A and 3B**), correlating with our recent observation of an erosion-like dissociation of CDDP/m in physiological conditions [28]. On the other hand, the scattering light intensities of Gluc-CDDP/m decreased to approximately 10% of the initial intensity after 96 h, and the decay profiles were comparable to that of CDDP/m (**Figure 3C**). In addition, the drug release rate of the series of micelles was evaluated by using the dialysis method under the same conditions of the stability experiments, *i.e.* 10 mM PBS plus 150 mM NaCl at 37 °C. The results showed that all the micelles have comparable drug release rate (**Figure 3D**). Therefore, glucose installation on CDDP/m did not affect the characteristics and behavior of the micelles in physiological conditions, allowing us to compare the different formulations in biological settings.

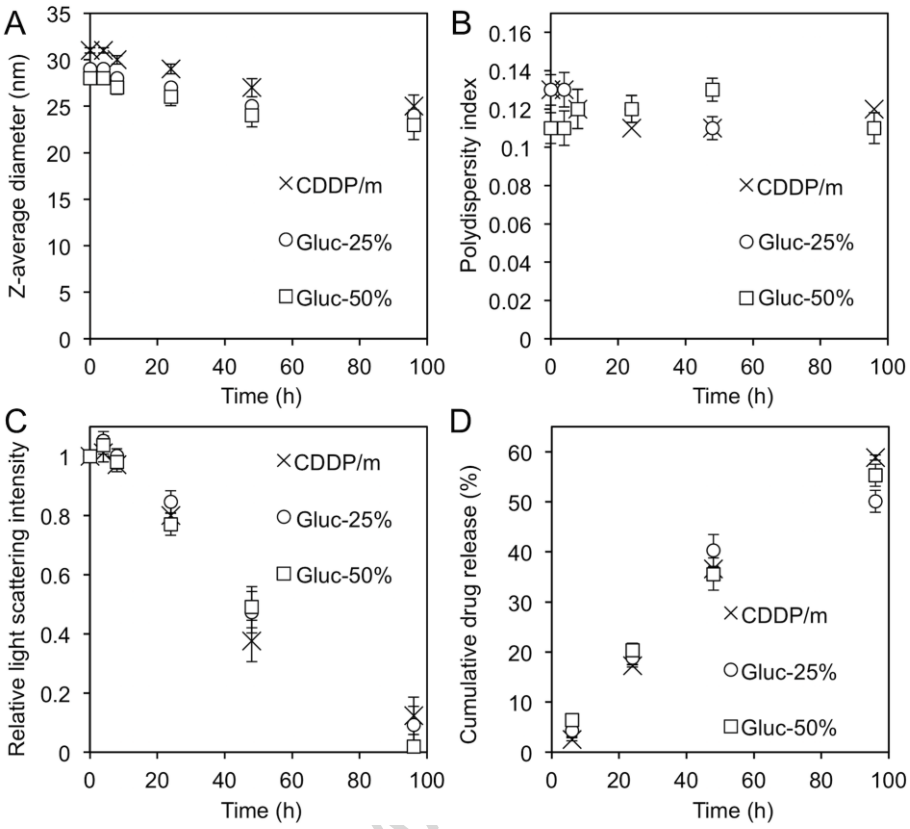

Figure 3. Stability and drug release rate of CDDP/m and Gluc-CDDP/m in 10 mM PBS plus 150 mM NaCl. A. Z-average diameter of the micelles. B. Polydispersity index (PDI). C. Relative light scattering intensity. D. Cumulative drug release. Data are shown as the mean ± S.D. (n = 3).

In vitro activity of glucose-installed cisplatin-loaded micelles

The biological activity of glucose-conjugated polymeric micelles was evaluated *in vitro* against three-dimensional multicellular spheroids, as spheroids offer significant advantages over monolayer cell culture for predicting *in vivo* efficacy, including the replication of several microenvironmental features of tumors, such as nutrient and oxygen supplies, drug gradients, three-dimensional multilayered cellular network, and intratumoral pH [32,33]. High-GLUT1-

expressing OSC-19 and low-GLUT1-expressing U87MG were selected for this study as cell lines with contrasting expression of GLUT1. The cells were incubated in spheroid microarray plates to form spheroids with 100-μm diameter, which were then incubated with free cisplatin and the series of polymeric micelles for 6 h, washed with fresh medium and post-incubated for 60 h. The results indicated that the Gluc-CDDP/m has a trend of higher cytotoxicity compared to CDDP/m against OCS-19 spheroids (**Figure 4; black bars**). These results indicate the importance of controlling the density of the glucose-ligand and the conjugation scheme for enhancing the activity of the micelles.

Knocking down GLUT1 on OCS19 cells (GLUT1(-) OCS19 cells) decreased the activity of the Gluc-CDDP/m against the OCS19 spheroids (**Figure 4; grey bars**). Moreover, in U87MG spheroids, the IC_{50} values for all the micelle systems were comparable regardless of the glucose functionalization and conjugation scheme (**Figure 4; white bars**). Thus, these results strongly suggest that the cytotoxicity of the Gluc-CDDP/m was mediated by GLUT1-targeting on the cancer cells. In addition, it is worth noting that even though the cell culture media used in these experiments contains high glucose concentration (4 g/L), the Gluc-CDDP/m showed enhanced cytotoxicity against OSC-19 spheroids.

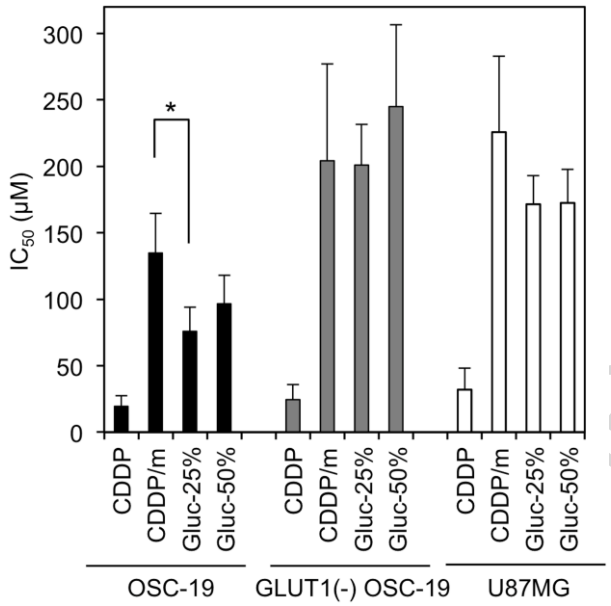

Figure 4. *In vitro* cytotoxicity of free CDDP, CDDP/m and Gluc-CDDP/m against multicellular spheroids of OSC-19 and U87MG cells. Data are shown as the mean ± S.D. (n = 4). *$p < 0.05$ determined by Student's t-test.

***In vivo* activity of glucose-installed cisplatin-loaded micelles**

The activity of free cisplatin and the series of CDDP/m was studied *in vivo* after systemically injecting into mice bearing subcutaneous OSC-19 tumors at 1 mg/kg on a cisplatin basis on days 0, 4, 8, and 11 (**Figure 5 A**). At day 36 after the start of the experiment, the volume of the tumors treated with Gluc-25%-CDDP/m was more than 3-fold smaller than that of the groups treated with free cisplatin and CDDP/m. Moreover, the Gluc-25%-CDDP/m was more effective than Gluc-50%-CDDP/m groups, indicating that the glucose conjugation scheme and the glucose density are critical for improving the efficacy. The significant antitumor activity of Gluc-25%-CDDP/m against OSC-19 tumors is also worthy of note, since these tumors are highly

resistant to CDDP, and present a large population of recalcitrant cancer cells with cancer stem-like cell properties [23]. The efficacy of the micelles was further studied in subcutaneous U87MG tumors, by following the same dosing and schedule as in the mice with OSC-19 tumors. Interestingly, despite the low GLUT1 expression of U87MG tumors (**Figure 2B**) [24], Gluc-25%-CDDP/m also inhibited the tumor growth more effectively than free cisplatin, CDDP/m, and Gluc-50%-CDDP/m (**Figure 5B**). Moreover, during the experiments, the body weight of mice remained unchanged, which indicated the safety of the treatments (**Figure 5C**).

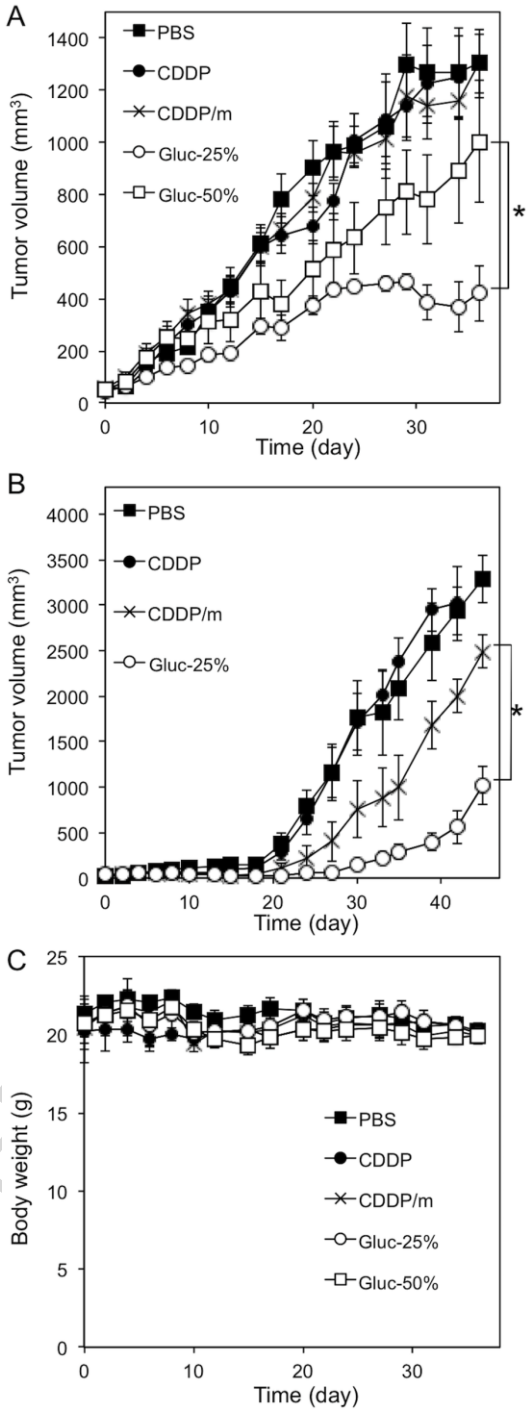

Figure 5. Antitumor activity of free CDDP and the series of micelles. A. OSC-19 tumors. B. U87MG tumors. C. Body weight changes during the antitumor activity experiment against OSC-19 tumors. The drugs were administered intravenously at 1 mg/kg on a cisplatin basis on days 0,

4, 8, and 11. Data are shown as the mean ± S.E.M (n = 6). *p < 0.05 determined by Student's t-test.

The activity enhancement of Gluc-25%-CDDP/m against these tumors suggests that it may present enhanced accumulation in the tumors compared to the other formulations. Thus, to confirm the contribution of the glucose ligands on the drug delivery efficiency, we evaluated the plasma clearance of free CDDP and the series of micelles, as well as their distribution in major organs and tumors (**Figure 6**). The amount of the injected dose present in the plasma and tissues was normalized to the total injected dose, *i.e.* 100 µg, and expressed as the % of injected dose per mL of plasma and g of tissue, respectively. The profiles of plasma clearance of CDDP/m and Gluc-25%-CDDP/m were comparable (**Figure 6A**) with approximately 88% dose/mL in plasma at 1 h after administration and 10% dose/mL at 24 h post-injection. The area under the plasma clearance curve ($AUC_{Plasma/0\text{-}24\ h}$) for Gluc-25%-CDDP/m was on part with that of CDDP/m (**Table 2**). Moreover, these tendencies are also in agreement with the plasma clearance of CDDP/m from our previous reports [27,28], indicating that the 25% modification of the PEG on the micelles with Gluc did not affect their blood circulation. Moreover, the comparable concentration of CDDP/m and Gluc-25%-CDDP/m in plasma suggests that Gluc-25%-CDDP/m did not undergo strong binding with GLUT1 on erythrocytes. On the other hand, increasing the density of Gluc to 50% decreased the level of the micelles in the bloodstream (**Figure 6A**). These results were also evident from the $AUC_{Plasma/0\text{-}24\ h}$ (**Table 2**), and indicate that the density of glucose on the micelles has significant effects on the clearance and bioavailability of the Gluc-CDDP/m.

The distribution of free CDDP and the micelles was also assessed in normal tissues, including liver, kidney, spleen, muscle, heart and brain, which express a wide range of glucose transporters [34]. In liver, Gluc-50%-CDDP/m displayed higher accumulation levels than CDDP/m at all the examined time points, whereas the accumulation of Gluc-25%-CDDP/m was comparable to that of CDDP/m (**Figure 6B**). The drop in the blood concentration of the micelles with 50% glucose correlated with their accumulation in liver, which was higher than that of the micelles having 0% and 25% glucose, suggesting that at 50% glucose installation, the micelles cannot overcome the liver barrier, leading to the drop in blood concentration. These observations are further supported by the area under the liver accumulation curves ($AUC_{Liver/0\text{-}24\,h}$) determined by trapezoidal rule (**Table 2**). These results indicate that appropriately tuning the glucose density on the micelles is key for overcoming the liver barrier, probably by reducing the interactions of Gluc-CDDP/m with the various GLUTs present in the intravascular compartment of liver [35], including GLUT1 in the sinusoidal membrane of hepatocytes, endothelial cells and Kupffer cells, GLUT2 in hepatocytes, GLUT3 in hepatocytes and GLUT4 in stellate cells. Moreover, the modification of the surface of the micelles with glucose did not affect their accumulation in kidney, spleen, muscle, heart and brain (**Figures 6C, 6D, 6E, 6F and 6G, respectively**), as all the micelles showed comparable low levels and AUCs (**Table 2**). The low accumulation of Gluc-CDDP/m to the brain, which was comparable to the minimal values observed for muscle, is particularly notable given the high expression of GLUT1 on the endothelium of the blood–brain barrier [36], and excludes any concern on off-target brain toxicities.

The accumulation of the micelles was also evaluated in both OSC-19 and U87MG xenografts. Accordingly, Gluc-25%-CDDP/m showed rapid accumulation in both tumors within 1-4 h after administration, and achieved intratumoral levels that doubled those of CDDP/m and

Gluc-50%-CDDP/m (**Figures 6H and 6I**). Also, the Gluc-50%-CDDP/m exerts higher accumulation than CDDP/m in OSC-19 tumors in the initial 4 h despite their short circulating time. Thus, while the accumulation profiles of CDDP/m in the tumors corresponded with the gradual extravasation in tumors usually observed for the EPR effect, the fast delivery of Gluc-25%-CDDP/m and Gluc-50%-CDDP/m into the tumors suggest an active transport mechanism. Notably, it has been reported that the U87MG glioblastoma model presents hypopermeable vasculature, which seriously limits the accumulation of nanomedicines [37]. Indeed, we have previously demonstrated that the EPR effect is restricted in U87MG tumors, where CDDP/m could only achieved around 3% of the injected dose per gram of tissue [8]. Interestingly, in this tumor model, the cRGD peptide installation on the surface of the micelles promoted their rapid vascular translocation in the initial 4 h [8], which is comparable to the fast accumulation of Gluc-25%-CDDP/m, suggesting a GLUT1 facilitated transvascular accumulation pathway. The area under the curves of the accumulation of drugs in tumors, *i.e.* $AUC_{OSC\text{-}19/0\text{-}24\ h}$ and $AUC_{U87MG/0\text{-}24\ h}$, showed that the exposure of Gluc-25%-CDDP/m to the tumors was more than 2-fold higher than for the other micelle formulations, and approximately 10-fold higher than free CDDP (**Table 2**).

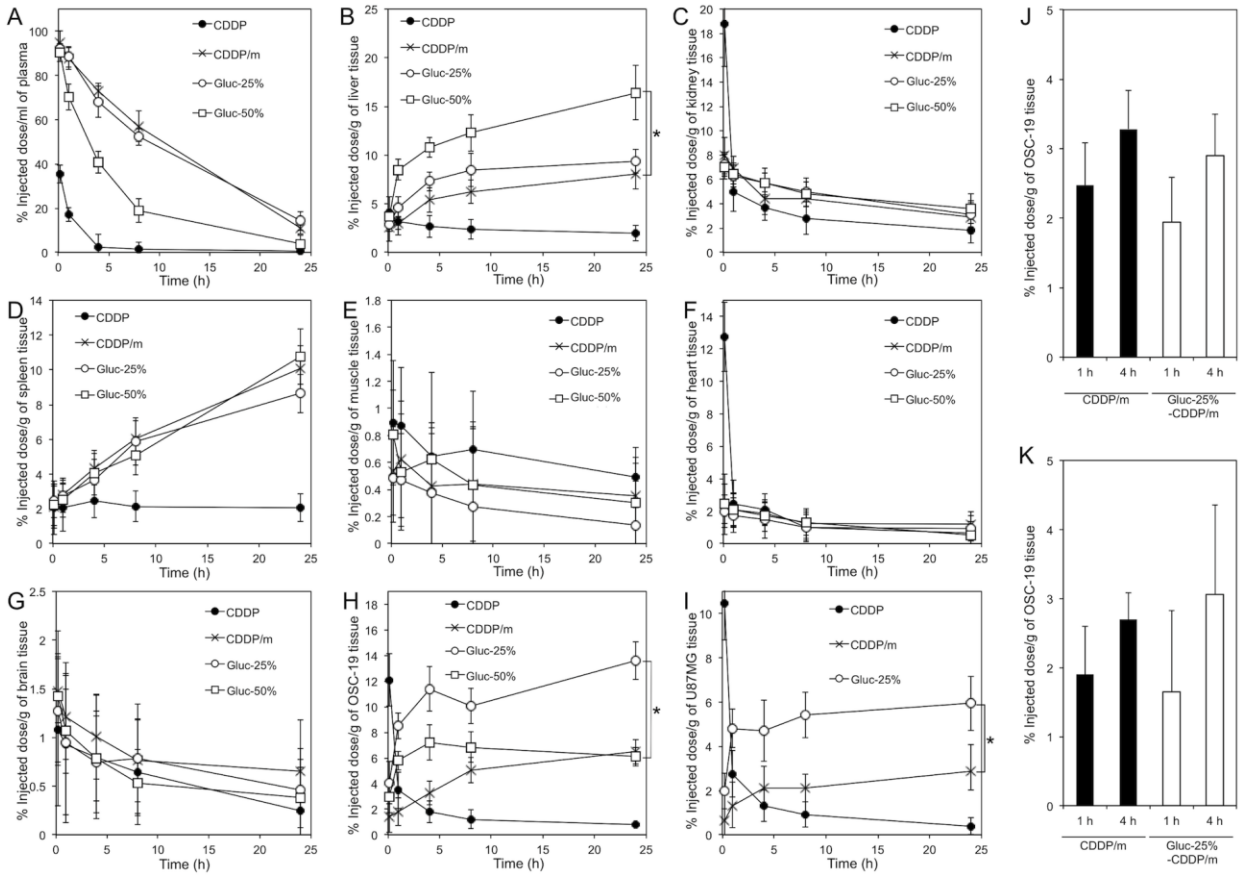

Figure 6. Biodistribution of free cisplatin, CDDP/m and Gluc-CDDP/m. A. Plasma. B. Liver. C. Kidney. D. Spleen. E. Muscle. F. Heart. G. Brain. H. OSC-19 tumors. I. U87MG tumors. Data are shown as the mean ± S.E.M (n = 6). *$p < 0.05$ determined by Student's t-test. J, K. Inhibition of the accumulation of Gluc-25% CDDP/m in OSC-19 tumors at 1 and 4 h after injection. J. Inhibition by intraperitoneal injection of glucose. K. Inhibition by intraperitoneal administration of the GLUT1-inhibitor STF-31. Data are shown as the mean ± S.D. (n = 6). CDDP/m were used as control.

The selective enhancement of the tumor accumulation of the Gluc-25%-CDDP/m was determined by calculating the ratio of the AUC in OSC-19 tumors ($AUC_{OSC\text{-}19/0\text{-}24\ h}$) and the

AUC in the organs (**Table 3**). The tumor/organ AUC ratios for Gluc-25%-CDDP/m were always higher than 1, demonstrating their selective accumulation enhancement in OSC-19 tumors.

Table 2. Area under the biodistribution curves (AUC) for free CDDP and the series of micelles[a]

Drug	AUC (%injected dose/g of tissue x h) ± S.E.M.								
	Plasma	Liver	Kidney	Spleen	Muscle	Heart	Brain	OSC-19	U87MG
Free CDDP	34.7 ± 39.1	51.9 ± 12.5	55.4 ± 16.4	50.9 ± 12.8	22.7 ± 11.7	13.3 ± 3.5	9.6 ± 8.5	25.7 ± 0.3	16.1 ± 2.5
CDDP/m	696.9 ± 43	172.2 ± 24.7	83.1 ± 21.5	200.5 ± 16.8	31.5 ± 12.2	9.2 ± 3.8	17.4 ± 9.9	135.2 ± 15.4	62.1 ± 18.7
Gluc-25%-CDDP/m	715.7 ± 70.1	209.8 ± 19.5	91.5 ± 16.1	175.2 ± 17.8	24.8 ± 12.2	4.8 ± 5.1	13.5 ± 11.6	298.8 ± 23.3*,**	134.7 ± 19.5*
Gluc-50%-CDDP/m	319.4 ± 60.5*	351.1 ± 44.5*	99.1 ± 19.8	206.3 ± 25.5	20.5 ± 9.1	8.8 ± 5.4	11.5 ± 5	151.6 ± 11.5	-

[a]Determined by trapezoidal rule.

* $p < 0.01$ compared to CDDP/m determined by Student's t-test.

** $p < 0.01$ compared to Gluc-50%-CDDP/m determined by Student's t-test.

Table 3. Ratio of the area under the biodistribution curves (AUC) between OSC-19 tumors and organs for free CDDP and the series of micelles

Drug	Tumor/Liver	Tumor/Kidney	Tumor/Spleen	Tumor/Muscle	Tumor/Heart	Tumor/Brain
Free CDDP	0.49	0.46	0.51	1.13	1.93	2.67
CDDP/m	0.78	1.63	0.67	4.29	14.69	7.77
Gluc-25%-CDDP/m	1.42	3.26	1.71	12.05	62.25	22.13
Gluc-50%-CDDP/m	0.43	1.53	0.73	7.39	17.22	13.18

To study the role of GLUT1 on the tumor accumulation of Gluc-25%-CDDP/m, we further evaluated the capacity of Gluc-25%-CDDP/m to accumulate in OSC-19 tumors in the presence of excess glucose, or the GLUT1 inhibitor STF-31 [38], as *in vivo* inhibition

experiments. Firstly, a 50 wt% glucose solution (200 μL) was intraperitoneally injected against OSC-19 tumor-bearing mice before and 30 min after micelle administration, and the changes in tumor accumulation of CDDP/m and Gluc-25%-CDDP/m were studied (**Figure 6J**). Thus, compared to the tumor accumulation obtained without glucose addition (normal condition in **Figure 6H**), the accumulation of Gluc-25%-CDDP/m decreased from 5.1% of injected dose/g of tissue to 2% of injected dose/g of tissue at 1 h after administration (**Figure 6J**; white bars), and from 8.3% of injected dose/g of tissue to 2.9% of injected dose/g of tissue at 4 h (**Figure 6J**; white bars). On the other hand, no changes in tumor accumulation of CDDP/m were observed at 1 and 4 h after administration (**Figure 6J**; black bars). Furthermore, GLUT1 was inactivated by intraperitoneally injecting STF-31 48 h, 24 h and 5 min (total three injections) before micelle administration. The accumulation enhancement of the glucose-installed micelles was again inhibited in a fashion comparable to the administration of excess glucose (**Figure 6K**; white bars), indicating that the interaction of the glucose moieties on the micelles with GLUT1 is fundamental for enhancing the tumor accumulation of Gluc-25%-CDDP/m.

Intravital observation of transvascular transport

To confirm the facilitated transport of Gluc-25%-CDDP/m into the tumors, we studied the accumulation process of the micelles by using intravital confocal laser scanning microscopy. Alexa647-labeled CDDP/m and Alexa555-labeled Gluc-25%-CDDP/m were mixed and co-injected intravenously to mice bearing OSC-19 tumors. The micelles were detected in the blood flow of the tumors just after injection (**Figure 7A**), with both Alexa647-labeled CDDP/m (**Figure 7A; red**) and Alexa555-labeled Gluc-25%-CDDP/m (**Figure 7A; green**) co-localizing within the blood vessels (**Figure 7A; yellow**). Thirty minutes after the injection of the micelles, the difference in their extravasation and tumor penetration behavior became evident, as the signal

from Alexa555-labeled Gluc-25%-CDDP/m in the interstitium of the tumor was much higher than the signal from Alexa647-labeled CDDP/m (**Figure 7A**). The quantification of the fluorescence profile of the micelles from the blood vessels into the tumor interstitium at 30 min clearly depicts the rapid extravasation and tumor penetration of Alexa555-labeled Gluc-25%-CDDP/m (**Figure 7B**). Moreover, the intensity of the Alexa555-labeled Gluc-25%-CDDP/m in the tumor interstitium increased faster than that of Alexa647-labeled CDDP/m (**Figure 7C**), which relates to the swift accumulation of Gluc-25%-CDDP/m detected in whole tumors (**Figure 6H**). These results confirmed the facilitated transvascular transport of Gluc-25%-CDDP/m into the tumors, showing for the first time that glucose-installed nanomedicines can be actively transported into tumors.

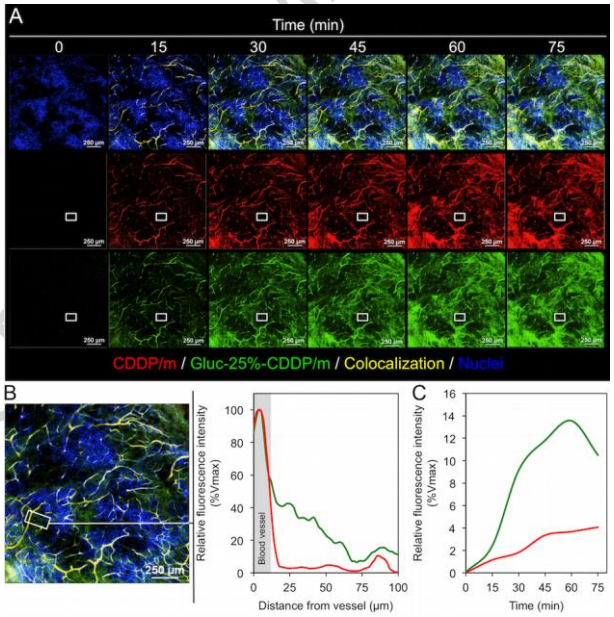

Figure 7. Real-time intravital microscopy of CDDP/m (Alexa647; red) and Gluc-25%-CDDP/m (Alexa555; green) in OSC-19 tumors. A. Time-lapse snapshots of the micelles in the tumors. B. Fluorescence profile from the blood vessels in the selected region of interest (ROI; white rectangle) into the tumor at 30 min after injection. The fluorescence intensity was normalized to

the maximum fluorescence attained in the blood vessels after injection. C. Fluorescence quantification at different time points in the selected ROIs (white rectangles in panel A). The cell nuclei were stained with Hoechst (blue). Scale bar = 250 μm.

DISCUSSION

Our results highlight the potential of precisely engineered glucose-installed nanomedicines for exploiting the GLUT1/glucose interaction toward enhancing their selective accumulation in tumors and promoting their efficacy. This was achieved through the controlled installation of glucose moieties on polymeric micelles, with appropriate conjugation through the carbon 6 and surface density (25% of the PEG chains). Thus, while the ability of Gluc-25%-CDDP/m to target aggressive GLUT1-expressing cancer cells improved their antitumor effects, the interaction of the Gluc-25%-CDDP/m with the GLUT1 on the tumor endothelium provided a transvascular pathway, which selectively increased intratumoral delivery. These findings suggest our strategy could be a promising approach for improving nanomedicine delivery to tumors beyond levels solely attained by the EPR effect.

The surface density of ligands is a critical parameter for adjusting the binding affinity of nanoparticle-based systems, as the increased number of ligands will prompt stronger multivalent interactions with the targets on the cells. Here, we used Gluc-25%- and Gluc-50%-CDDP/m, and observed that having a glucose density of 50% on the micelles neither improved the *in vitro* efficacy in OSC-19 spheroids, nor enhanced the drug levels in the tumors *in vivo*, indicating the importance of engineering the density of glucose moieties on the micelles. Moreover, Gluc-50%-CDDP/m showed higher accumulation than Gluc-25%-CDDP/m in liver. Such differences between Gluc-25%-CDDP/m and Gluc-50%-CDDP/m could be associated with a tighter

multivalent binding of the Gluc-50%-CDDP/m to a number of GLUT1 molecules expressing on the cellular surface compared to Gluc-25%-CDDP/m, which may facilitate the retention of the former in liver and reduce the transvascular transport of Gluc-50%-CDDP/m into tumors. We have previously studied such multivalency effect by surface plasmon resonance using lactose-installed polymeric micelles [39]. This study confirmed that the multivalent binding of the micelles accelerated the association phase and slowed the dissociation phases. Moreover, the multivalent bonding has been previously observed for a wide range of nanoparticles and supramolecular systems modified with ligands, such as cRGD peptide [40-42]. In fact, we previously observed a comparable effect of cRGD ligands on nanocarriers, where the strong integrin binding at high ligand densities promoted the retention in liver and impaired the extravasation in tumors [42]. In addition, while the effect of modifying the micelles with glucose densities between the 25-50% range has not been explored, it is likely that there is an optimal glucose density for selectively increasing the accumulation in the tumor, while overcoming the liver barrier. While such optimization is beyond the scope of this study, our conclusion that the density of glucose should be carefully engineered to promote tumor accumulation and avoid the sequestration in the organs is supported by the findings with 0%, 25% and 50% glucose densities.

The expression of GLUT receptors throughout the body could be considered a potential source for off-target effects even for engineered glucose-conjugated nanomedicines, as there are at least 12 types of GLUT transporters in the body, including GLUT1 in erythrocytes and the blood-brain barrier, as well as ubiquitously expressed for basal-level glucose uptake, GLUT2 in hepatocytes, intestines, kidney and β-pancreatic cells, GLUT3 in neurons, sperm and circulating white blood cells, and insulin-triggered GLUT4 in adipocytes and muscles [14,34].

Nevertheless, the interaction of the micelles with GLUTs expressed on interstitial cells may be restricted, as the relatively large size of polymeric micelles prevents their extravasation into healthy tissues due to the upper limits of the pore size for transvascular flow across the different endothelial layers [43]. For example, 1-nm upper limit for non-sinusoidal non-fenestrated blood capillaries, such as those in the brain, 5-nm for capillaries having clefts lined with macula occludens junctions, such as the capillaries of skeletal muscle, 6-12 nm for non-sinusoidal fenestrated blood capillaries with diaphragmed fenestrae, such as the vessels in exocrine glands, and 15-nm for capillary walls of non-sinusoidal fenestrated capillaries with open fenestrae, such as the kidney glomeruli [43]. The comparable levels of Gluc-25%-CDDP/m and CDDP/m in plasma and organs verify the aforesaid observation, and demonstrate that the GLUT1 targeting ability of the micelles did not lead to an off-target distribution. Moreover, the Gluc-25%-CDDP/m selectively accumulated in tumor, as confirmed by the AUC ratio between the OSC19 tumors and the organs, which was always higher than 1. Such high tumor selectivity of Gluc-25%-CDDP/m allowed promoting the therapeutic efficacy without toxicity.

The GLUT1 on endothelial cells controls the passage of glucose through vascular barriers, such as the blood-brain barrier or the blood-retinal barrier [20,21,44]. Our immunofluorescence study also showed the presence of GLUT1 on the malignant vasculature, conceivably accounting for the import of glucose into the tumors. On the other hand, it should be pointed that, while GLUT1 can readily deliver small glucose molecules through facilitated diffusion, large macromolecular glucose-conjugates cannot pass across GLUT1. Nevertheless, our previous report showed that the extravasation of glucose-installed micelles through the blood-brain barrier into the brain parenchyma was significantly enhanced by the regulation of the subcellular localization of GLUT1 by glycaemic control, as follows: after a period of fasting,

high-levels of GLUT1 were located on the luminal side of brain endothelial cells, which enhanced the binding to glucose-installed micelles circulating in the bloodstream. Then, an intraperitoneal administration of glucose triggered the recycling of the GLUT1 to the abluminal side of the brain endothelial cells, carrying the glucose-installed micelles into the brain parenchyma [45]. On the other hand, in the case of OSC-19 and U87MG tumors, Gluc-25%-CDDP/m were translocated into the tumor interstitium without the assistance of a glycaemic control, while the brain accumulation of the micelles remained low, excluding potential toxicities to the brain at normal conditions without fasting and glycemic control. This GLUT1-facilitated transport in tumors could be associated with the increased levels and subcellular localization of GLUT1 on the endothelial cells of tumors due to the alterations in metabolic homeostasis, such as nutrient or oxygen deprivation, or extracellular signals promoting cell growth and proliferation [46-53]. For example, hypoxia, which is a hallmark of malignancy, has been shown to increase GLUT1 expression in the luminal side of endothelial cells [46-49]. Moreover, the GLUT1 position on cells is being continuously adjusted according to metabolic demands, shifting from internal vesicular compartments to the cell surfaces, and *vice versa* [50-53]. Such perturbations in the GLUT1 expression, activity and location due to the altered metabolism may also explain the selective and rapid enhancement of the accumulation of Gluc-25%-CDDP/m into the tumors compared to the healthy organs.

Solid tumors usually present insufficient supply of oxygen, activating the hypoxia inducible factor-1 (HIF-1) pathway, which prompts an adaptive response on genes that regulate glycolytic metabolism, promoting glucose uptake through the transcription of GLUTs [54]. Increasing evidence indicates that such glucose metabolism is even higher in cancer stem-like cells (CSCs), *i.e.* a sub-population of drug-resistant cancer cells with self-renewal and

tumorigenic capabilities, with hypoxic regions in tumors serving as specialized niches for CSC maintenance and GLUT1 having a central role in the stemness, growth and survival of CSCs [55-58]. In fact, GLUT1 expression in tumors has been associated with tumor malignancy and resistance to therapies [16,58], including CDDP resistance in head and neck tumors [23,60-62]. The CSCs in head and neck tumors have been identified as the cellular fraction expressing variant isoforms of CD44 (CD44v), which show high GLUT1 and high cytosolic levels of glutathione that permanently inactivate CDDP [23]. Our previous reports showed that CDDP/m can avoid the glutathione detoxification by increased drug delivery to the nucleus of human oral squamous cell carcinoma HSC-2 cells, which display a large fraction of CD44v-positive CSCs, effectively overcoming drug resistance [63,64]. In current study, we evaluated the antitumor activity against OSC-19 tumors, which have an even larger CD44v-positive sub-population than HSC-2 cells, and are approximately 4-fold more resistant to CDDP than HSC-2 cells [23]. Thus, the activity of CDDP/m was insufficient to suppress the growth of OSC-19 tumors. On the other hand, Gluc-25%-CDDP/m effectively reduced the tumor growth rate, suggesting that the GLUT1-targeting could synergize with the ability of CDDP/m for surmounting drug resistance by increasing the drug levels in tumors, as well as enhancing the activity against GLUT1-expressing cancer cells. Such activity enhancement indicates GLUT1-targeting as an attractive approach for developing therapies against drug resistant tumors.

CONCLUSION

By developing glucose-installed polymeric micelles having the glucose ligands conjugated *via* the carbon 6 and an engineered ligand density of 25%, we successfully targeted the GLUT1 on the tumor vasculature and on cancer cells, promoting the selective accumulation

of the micelles in tumors and enhancing their antitumor activity, even against drug resistant tumors. Targeting the GLUT1 on the tumor vascular endothelium effectively facilitated the translocation of the micelles from the blood compartment into the tumor interstitium, doubling the accumulation levels achieved solely by the EPR effect. Thus, while highly specific markers against tumors are being considered for tumor targeting and emplacement on nanomedicines, which would increase complexity and personalization of therapies due to the heterogeneous nature of cancer, our findings will contribute to drive the development of comprehensive nanomedicine systems capable of targeting tumors through simple glucose biochemistry. Given the glycolytic demands of a wide range of tumors, and its connection with tumor malignancy and drug resistance, our approach has the potential for developing broadly applicable therapeutic strategies against aggressive cancers.

ACKNOWLEDGEMENTS

This research was supported by the Center of Innovation Science and Technology based Radical Innovation and Entrepreneurship Program (COI STREAM; KK) from the Ministry of Education, Culture, Sports, Science and Technology (MEXT), the Practical Research for Innovative Cancer Control from Japan Agency for Medical Research and Development (AMED), the Project for Development of Innovative Research on Cancer Therapeutics (P-DIRECT) from AMED. This work was also partially supported by Grants-in-Aid for Scientific Research B (JP16H03179; H.C.) from the Japan Society for the Promotion of Science (JSPS), the Project for Cancer Research And Therapeutic Evolution (P-CREATE) (JP17cm0106202; H.C. and K.K.) from Japan Agency for Medical Research and Development (AMED).

REFERENCES

1. Y. Matsumura, H Maeda, A New Concept for Macromolecular Therapeutics in Cancer Chemotherapy: Mechanism of Tumoritropic Accumulation of Proteins and the Antitumor Agent SMANCS, Cancer Res. 46 (1986) 6387-6392.

2. H. Maeda, K. Tsukigawa, J. Fang, A Retrospective 30 Years After Discovery of the Enhanced Permeability and Retention Effect of Solid Tumors: Next-Generation Chemotherapeutics and Photodynamic Therapy-Problems, Solutions, and Prospects, Microcirculation 23 (2016) 173-182.

3. Y.H. Bae, K. Park, Targeted Drug Delivery to Tumors: Myths, Reality and Possibility, J. Control. Release 153 (2011) 198-205.

4. R.K. Ramanathan, R.L. Korn, N. Raghunand, J.C. Sachdev, R.G. Newbold, G. Jameson, G.J. Fetterly, J. Prey, S.G. Klinz, J. Kim, J. Cain, B.S. Hendriks, D.C. Drummond, E. Bayever, J.B. Fitzgerald, Correlation between Ferumoxytol Uptake in Tumor Lesions by MRI and Response to Nanoliposomal Irinotecan in Patients with Advanced Solid Tumors: A Pilot Study, Clin. Cancer Res. 23 (2017) 3638-3648.

5. H. Lee, A.F. Shields, B.A. Siegel, K.D. Miller, I. Krop, C.X. Ma, P.M. LoRusso, P.N. Munster, K. Campbell, D.F. Gaddy, S.C. Leonard, E. Geretti, S.J. Blocker, D.B. Kirpotin, V. Moyo, T.J. Wickham, B.S. Hendriks, ^{64}Cu-MM-302 Positron Emission Tomography Quantifies Variability of Enhanced Permeability and Retention of Nanoparticles in Relation to Treatment Response in Patients with Metastatic Breast Cancer, Cancer Res. 23 (2017) 4190-4202.

6. A. Nel, E. Ruoslahti, H. Meng, New Insights into "Permeability" as in the Enhanced Permeability and Retention Effect of Cancer Nanotherapeutics, ACS Nano 11 (2017) 9567-9569.

7. H. Cabral, K. Miyata, K. Osada, K. Kataoka, Block Copolymer Micelles in Nanomedicine Applications, Chem. Rev. 118 (2018) 6844-6892.

8. Y. Miura, T. Takenaka, K. Toh, S. Wu, H. Nishihara, M.R. Kano, Y. Ino, T. Nomoto, Y. Matsumoto, H. Koyama, H. Cabral, N. Nishiyama, K. Kataoka, Cyclic RGD-Linked Polymeric Micelles for Targeted Delivery of Platinum Anticancer Drugs to Glioblastoma through the Blood–Brain Tumor Barrier, ACS Nano 7 (2013) 8583-8592.

9. S. Quader, X. Liu, Y. Chen, P. Mi, T. Chida, T. Ishii, Y. Miura, N. Nishiyama, H. Cabral, K. Kataoka, cRGD Peptide-Installed Epirubicin-Loaded Polymeric Micelles for Effective Targeted Therapy against Brain Tumors, J. Control. Release 258 (2017) 56-66.

10. E. Ruoslahti, Tumor Penetrating Peptides for Improved Drug Delivery, Adv. Drug Deliv. Rev. 110-111 (2017) 3-12.

11. D. Hanahan, R.A. Weinberg. Hallmarks of Cancer: The Next Generation, Cell 144 (2011) 646-674.

12. N.N. Pavlova, C.B. Thompson, The Emerging Hallmarks of Cancer Metabolism, Cell Metabolism 23 (2016) 27-47.

13. M.G. Vander Heiden, Targeting Cancer Metabolism: A Therapeutic Window Opens, Nat. Rev. Drug Discov. 10 (2011) 671-684.

14. R.A. Medina, G.I. Owen, Glucose Transporters: Expression, Regulation and Cancer, Biol. Res. 35 (2002) 9-26.

15. M. Yu, H. Yongzhi, S. Chen1, X. Luo, Y. Lin, Y. Zhou, H. Jin, B. Hou, Y. Deng, L. Tu, Z. Jian, The Prognostic Value of GLUT1 in Cancers: A Systematic Review and Meta-analysis, Oncotarget 8 (2017) 43356-43367.

16. P.B. Ancey, C. Contat, E. Meylan, Glucose Transporters in Cancer – From Tumor Cells to the Tumor Microenvironment, FEBS J. 285 (2018) 2926-2943.

17. E. C. Calvaresia, P. J. Hergenrother, Glucose Conjugation for the Specific Targeting and Treatment of Cancer, Chem. Sci. 4 (2013) 2319-2333.

18. R.K. Tekade, X. Sun, The Warburg Effect and Glucose-Derived Cancer Theranostics, Drug Discov. Today 22 (2017) 1637-1653.

19. X. Jiang, H. Xin, Q. Ren, J. Gu, L. Zhu, F. Du, C. Feng, Y. Xie, X. Sha, X. Fang. Nanoparticles of 2-Deoxy-D-Glucose Functionalized Poly(ethylene glycol)-co-Poly(trimethylene carbonate) for Dual-Targeted Drug Delivery in Glioma Treatment, Biomaterials 25 (2014) 518-529

20. A.P. Dick, S.I. Harik, A. Klip, D.M. Walker, Identification and Characterization of the Glucose Transporter of the Blood-Brain Barrier by Cytochalasin B Binding and Immunological Reactivity, Proc. Natl. Acad. Sci. U.S.A. 81 (1984) 7233-7237.

21. A.L. Olson, J.E. Pessin, Structure, Function, and Regulation of the Mammalian Facilitative Glucose Transporter Gene Family, Annu. Rev. Nutr. 16 (1996) 235-256

22. H. Cabral, K. Kataoka, Progress of Drug-Loaded Polymeric Micelles into Clinical Studies, J. Control. Release 190 (2014) 465-476.

23. M. Yoshikawa, K. Tsuchihashi, T. Ishimoto, T. Yae, T. Motohara, E. Sugihara, N. Onishi, T. Masuko, K. Yoshizawa, S. Kawashiri, M. Mukai, S. Asoda, H. Kawana, T. Nakagawa, H. Saya, O. Nagano, xCT Inhibition Depletes CD44v-Expressing Tumor Cells that Are Resistant to EGFR-Targeted Therapy in Head and Neck Squamous Cell Carcinoma, Cancer Res. 73 (2013) 1855-1866.

24. Q. Jin, L. Agrawal, Z. Vanhorn-Ali, G. Alkhatib, GLUT-1-independent infection of the glioblastoma/astroglioma U87 cells by the human T cell leukemia virus type 1, Virology 353 (2006) 99-110.

25. M. Szwarc, M. Levy, R. Milkovich, Polymerization Initiated by Electron Transfer to Monomer. A New Method of Formation of Block Polymers, J. Am. Chem. Soc. 78 (1956) 2656.

26. T. Nakamura, Y. Nagasaki, K. Kataoka, Synthesis of Heterobifunctional Poly(ethylene glycol) with a Reducing Monosaccharide Residue at One End, Bioconjugate Chem. 9 (1998) 300-303.

27. N. Nishiyama, S. Okazaki, H. Cabral, M. Miyamoto, Y. Kato, Y. Sugiyama, K. Nishio, Y. Matsumura, K. Kataoka, Novel Cisplatin-Incorporated Polymeric Micelles Can Eradicate Solid Tumors in Mice, Cancer Res. 63 (2003) 8977-8983.

28. Y. Mochida, H. Cabral, Y. Miura, F. Albertini, S. Fukushima, K. Osada, N. Nishiyama, K. Kataoka, Bundled Assembly of Helical Nanostructures in Polymeric Micelles Loaded with

Platinum Drugs Enhancing Therapeutic Efficiency against Pancreatic Tumor, ACS Nano 8 (2014) 11591-11602.

29. Y. Matsumoto, T. Nomoto, H. Cabral, Y. Matsumoto, S. Watanabe, R.J. Christie, K. Miyata, M. Oba, T. Ogura, Y. Yamasaki, N. Nishiyama, T. Yamasoba, K. Kataoka, Direct and Instantaneous Observation of Intravenously Injected Substances Using Intravital Confocal Micro-Videography, Biomed. Opt. Express 1 (2010) 1209-1216.

30. J.E. Barnett, G.D. Holman, K.A. Munday, Structural Requirements for Binding to the Sugar-Transport System of the Human Erythrocyte, Biochem J. 131 (1973) 211-221.

31. M. Mueckler, C. Makepeace, Model of the Exofacial Substrate-Binding Site and Helical Folding of the Human Glut1 Glucose Transporter Based on Scanning Mutagenesis, Biochemistry 48 (2009) 5934-5942.

32. R.M. Sutherland, Cell and Environment Interactions in Tumor Microregions: The Multicell Spheroid Model. Science 240 (1988) 177-184.

33. M. Zanoni, F. Piccinini, C. Arienti, A. Zamagni, S. Santi, R. Polico, A. Bevilacqua, A. Tesei, 3D Tumor Spheroid Models for In Vitro Therapeutic Screening: A Systematic Approach to Enhance the Biological Relevance of Data Obtained, Sci. Rep. 6 (2016) Article number: 19103.

34. B. Thorens, M. Mueckler, Glucose Transporters in the 21st Century, Am. J. Physiol. Endocrinol. Metab. 298 (2010) E141-E145

35. S. Karim, D.H. Adams, P.F. Lalor, Hepatic Expression and Cellular Distribution of the Glucose Transporter Family, World J. Gastroenterol. 18 (2012) 6771

36. W.M. Pardridge, R.J. Boado, C.R. Farrell, Brain-Type Glucose Transporter (GLUT-1) is Selectively Localized to the Blood-Brain Barrier. Studies with Quantitative Western Blotting and In Situ Hybridization, J. Biol. Chem. 265 (1990) 18035-18040

37. S.K. Hobbs, W.L. Monsky, F. Yuan, W.G. Roberts, L. Griffith, V.P. Torchilin, R.K. Jain, Regulation of Transport Pathways in Tumor Vessels: Role of Tumor Type and Microenvironment, Proc. Natl. Acad. Sci. U.S.A. 95 (1998) 4607-4612

38. D.A. Chan, P.D. Sutphin, P. Nguyen, S. Turcotte, E.W. Lai, A. Banh, G.E. Reynolds, J.-T. Chi, J. Wu, D.E. Solow-Cordero, M. Bonnet, J.U. Flanagan, D.M. Bouley, E.E. Graves, W.A. Denny, M.P. Hay, A.J. Giaccia, Targeting GLUT1 and the Warburg Effect in Renal Cell Carcinoma by Chemical Synthetic Lethality, Sci Transl Med 3 (2011) 94ra70.

39. E. Jule, Y. Nagasaki, K. Kataoka, Lactose-Installed Poly(ethylene glycol)−Poly(d,l-lactide) Block Copolymer Micelles Exhibit Fast-Rate Binding and High Affinity toward a Protein Bed Simulating a Cell Surface. A Surface Plasmon Resonance Study, Bioconjugate Chem. 14 (2003) 177–186.

40. H. Kubas, M. Schäfer, U. Bauder-Wüst, M. Eder, D. Oltmanns, U. Haberkorn, W. Mier, M. Eisenhut, Multivalent cyclic RGD ligands: influence of linker lengths on receptor binding, Nuclear Med. Biol. 37 (2010) 885-891.

41. X. Montet, M. Funovics, K. Montet-Abou, R. Weissleder, L. Josephson, Multivalent Effects of RGD Peptides Obtained by Nanoparticle Display, J. Med. Chem. 49 (2006) 6087–6093.

42. W. Kawamura, Y. Miura, D. Kokuryo, K. Toh, N. Yamada, T. Nomoto, Y. Matsumoto, D. Sueyoshi, X. Liu, I. Aoki, M. R. Kano, N. Nishiyama, T. Saga, A. Kishimura, K. Kataoka,

Density-Tunable Conjugation of Cyclic RGD Ligands with Polyion Complex Vesicles for the Neovascular Imaging of Orthotopic Glioblastomas. Sci. Technol. Adv. Mater. 16 (2015) 035004.

43. H. Sarin, Physiologic Upper Limits of Pore Size of Different Blood Capillary Types and Another Perspective on the Dual Pore Theory of Microvascular Permeability, J. Angiogenes. Res. 2 (2010) 14.

44. K. Takata, T. Kasahara, M. Kasahara, O. Ezaki, H. Hirano, Ultracytochemical Localization of the Erythrocyte/HepG2-type Glucose Transporter (GLUT1) in Cells of the Blood-Retinal Barrier in the Rat, Invest. Ophthalmol. Vis. Sci. 33 (1992) 377-383.

45. Y. Anraku, H. Kuwahara, Y. Fukusato, A. Mizoguchi, T. Ishii, K. Nitta, Y. Matsumoto, K. Toh, K. Miyata, S. Uchida, K. Nishina, K. Osada, K. Itaka, N. Nishiyama, H. Mizusawa, T. Yamasoba, T. Yokota, K. Kataoka, Glycaemic Control Boosts Glucosylated Nanocarrier Crossing the BBB into the Brain, Nat. Commun. 8 (2017) 1001.

46. J.Z. Zhang, A. Behrooz, F. Ismail-Beigi, Regulation of Glucose Transport by Hypoxia, Am J Kidney Dis 34 (1999) 189-202.

47. S.J. Vannucci, R. Reinhart, F. Maher, C.A. Bondy, W.H. Lee, R.C. Vannucci, I.A. Simpson, Alterations in GLUT1 and GLUT3 Glucose Transporter Gene Expression Following Unilateral Hypoxia-Ischemia in the Immature Rat Brain, Brain Res. 107 (1998) 255-264.

48. A.K. Kumagai, S.A. Vinores, W.M. Pardridge, Pathological Upregulation of Inner Blood-Retinal Barrier Glut1 Glucose Transporter Expression in Diabetes Mellitus, Brain Res. 706 (1996) 313-317.

49. S.I. Harik, R.A. Behmand, J.C. LaManna, Hypoxia Increases Glucose Transport at Blood-Brain Barrier in Rats, J. Appl. Physiol. 77 (1994) 896-901.

50. S.A. Baldwin, L.F. Barros, M. Griffiths, Trafficking of Glucose Transporters-Signals and Mechanisms, Biosci. Rep. 15 (1995) 419-426.

51. H.L. Wieman, J.A. Wofford, J.C. Rathmell, Cytokine Stimulation Promotes Glucose Uptake via Phosphatidylinositol-3 Kinase/Akt Regulation of Glut1 Activity and Trafficking, Mol Biol Cell 18 (2007) 1437-1446.

52. C. Zhang, J. Liu, Y. Liang, R. Wu, Y. Zhao, X. Hong, M. Lin, H. Yu, L. Liu, A.J. Levine, W. Hu, Z. Feng, Tumour-Associated Mutant p53 Drives the Warburg Effect, Nat. Commun. 4 (2013) 2935.

53. S.R. Shinde, S. Maddika, PTEN Regulates Glucose Transporter Recycling by Impairing SNX27 Retromer Assembly, Cell Rep. 21(2017) 1655-1666.

54. G.L. Semenza, Targeting HIF-1 for Cancer Therapy, Nat. Rev. Cancer 3 (2003) 721-732.

55. Z. Li, S. Bao, Q. Wu, H. Wang, C. Eyler, S. Sathornsumetee, Q. Shi, Y. Cao, J. Lathia, R.E. McLendon, A.B. Hjelmeland, J.N. Rich, Hypoxia-Inducible Factors Regulate Tumorigenic Capacity of Glioma Stem Cells, Cancer Cell 15 (2009) 501-513.

56. Zhou Y1, Zhou Y, Shingu T, Feng L, Chen Z, Ogasawara M, Keating MJ, Kondo S, Huang P.

57. Y. Zhou, Y. Zhou, T. Shingu, L. Feng, Z. Chen, M. Ogasawara, M.J. Keating, S. Kondo, P. Huang, Metabolic Alterations in Highly Tumorigenic Glioblastoma Cells: Preference for Hypoxia and High Dependency on Glycolysis, J Biol Chem. 286 (2011) 32843-32853.

58. K. Shibuya, M. Okada, S. Suzuki, M. Seino, S. Seino, H. Takeda, C. Kitanaka, Targeting the Facilitative Glucose Transporter GLUT1 Inhibits the Self-Renewal and Tumor-Initiating Capacity of Cancer Stem Cells. Oncotarget 6 (2015) 651-661.

59. M. Yu, H. Yongzhi, S. Chen, X. Luo, Y. Lin, Y. Zhou, H. Jin, B. Hou, Y. Deng, L. Tu, Z. Jian, The Prognostic Value of GLUT1 in Cancers: A Systematic Review and Meta-analysis. Oncotarget 8 (2017) 43356-43367

60. S.-J. Li, X.-N. Yang, H.-Yu. Qian, Antitumor Effects of WNT2B Silencing in GLUT1 Overexpressing Cisplatin Resistant Head and Neck Squamous Cell Carcinoma, Am. J. Cancer Res. 5 (2015) 300-308.

61. M. Shimanishi, K. Ogi, Y. Sogabe, T. Kaneko, H. Dehari, A. Miyazaki, H. Hiratsuka, Silencing of GLUT-1 Inhibits Sensitization of Oral Cancer Cells to Cisplatin During Hypoxia, J. Oral Pathol. Med. 42 (2013) 382-388.

62. S. Li, X. Yang, P. Wang, X. Ran, The Effects of GLUT1 on the Survival of Head and Neck Squamous Cell Carcinoma, Cell Physiol. Biochem. 32 (2013) 624-634.

63. M. Wang, Y Miura, K Tsuchihashi, K Miyano, O Nagano, M Yoshikawa, A. Tanabe, J. Makino, Y. Mochida, N. Nishiyama, H. Saya, H. Cabral, K. Kataoka, Eradication of CD44-Variant Positive Population in Head and Neck Tumors through Controlled Intracellular Navigation of Cisplatin-Loaded Nanomedicines, J. Control. Release 230 (2016) 26-33.

64. K. Miyano, H. Cabral, Y. Miura, Y. Matsumoto, Y. Mochida, H. Kinoh, C. Iwata, O. Nagano, H. Saya, N. Nishiyama, K. Kataoka, T. Yamasoba, cRGD Peptide Installation on Cisplatin-Loaded Nanomedicines Enhances Efficacy against Locally Advanced Head and Neck Squamous Cell Carcinoma bearing Cancer Stem-Like Cells, J. Control. Release 261(2017) 275-286.

GRAPHICAL ABSTRACT